Monthly Notices
of the
ROYAL ASTRONOMICAL SOCIETY

MNRAS **430,** 1566–1577 (2013) doi:10.1093/mnras/sts680

Mining the *Herschel*-Astrophysical Terahertz Large Area Survey: submillimetre-selected blazars in equatorial fields

M. López-Caniego,[1⋆] J. González-Nuevo,[1] M. Massardi,[2] L. Bonavera,[1] D. Herranz,[1] M. Negrello,[3] G. De Zotti,[3,4] F. J. Carrera,[1] L. Danese,[4] S. Fleuren,[5] M. Hardcastle,[6] M. J. Jarvis,[6,7] H.-R. Klöckner,[8,9] T. Mauch,[6] P. Procopio,[10] S. Righini,[2] W. Sutherland,[5] R. Auld,[11] M. Baes,[12] S. Buttiglione,[3] C. J. R. Clark,[11] A. Cooray,[13] A. Dariush,[14] L. Dunne,[15] S. Dye,[16] S. Eales,[11] R. Hopwood,[14,17] C. Hoyos,[16] E. Ibar,[18] R. J. Ivison,[18,19] S. Maddox[15] and E. Valiante[11]

[1] *Instituto de Física de Cantabria (CSIC-UC), Avda. los Castros s/n, E-39005 Santander, Spain*
[2] *INAF – Istituto di Radioastronomia, Via P. Gobetti n. 101, I-40129 Bologna, Italy*
[3] *INAF – Osservatorio Astronomico di Padova, Vicolo dell'Osservatorio 5, I-35122 Padova, Italy*
[4] *Astrophysics Sector, SISSA, Via Bonomea 265, I-34136 Trieste, Italy*
[5] *School of Physics and Astronomy, Queen Mary University of London, Mile End Road, London E1 4NS, UK*
[6] *Centre for Astrophysics Research, STRI, University of Hertfordshire, Hatfield AL10 9AB, UK*
[7] *Physics Department, University of the Western Cape, Private Bag X17, Bellville 7535, South Africa*
[8] *University of Oxford, Denys Wilkinson Building, Oxford OX1 3RH, UK*
[9] *Max-Planck-Institut für Radioastronomie, Auf dem Hügel 69, D-53121 Bonn, Germany*
[10] *School of Physics, David Caro Building, Corner of Tin Alley and Swanston St, The University of Melbourne, Parkville, VIC 3010, Australia*
[11] *School of Physics and Astronomy, Cardiff University, The Parade, Cardiff CF24 3AA, UK*
[12] *Sterrenkundig Observatorium, Universiteit Gent, Krijgslaan 281 S9, B-9000 Gent, Belgium*
[13] *Department of Physics and Astronomy, University of California, Irvine, CA 92697, USA*
[14] *Department of Physics, Imperial College London, South Kensington Campus, London SW7 2AZ, UK*
[15] *Department of Physics and Astronomy, University of Canterbury, Private Bag 4800, Christchurch 8140, New Zealand*
[16] *School of Physics and Astronomy, University of Nottingham, University Park, Nottingham NG7 2RD, UK*
[17] *Department of Physical Sciences, The Open University, Milton Keynes MK7 6AA, UK*
[18] *UK Astronomy Technology Centre, Royal Observatory, Blackford Hill, Edinburgh EH9 3HJ, UK*
[19] *Institute for Astronomy, University of Edinburgh, Royal Observatory, Edinburgh EH9 3HJ, UK*

Accepted 2012 December 20. Received 2012 December 17; in original form 2012 May 9

ABSTRACT

The *Herschel*-Astrophysical Terahertz Large Area Survey (H-ATLAS) provides an unprecedented opportunity to search for blazars at sub-mm wavelengths. We cross-matched the Faint Images of the Radio Sky at Twenty-cm (FIRST) radio source catalogue with the 11 655 sources brighter than 35 mJy at 500 μm in the ∼135 deg^2 of the sky covered by the H-ATLAS equatorial fields at 9^h and 15^h, plus half of the field at 12^h. We found that 379 of the H-ATLAS sources have a FIRST counterpart within 10 arcsec, including eight catalogued blazars (plus one known blazar that was found at the edge of one of the H-ATLAS maps). To search for additional blazar candidates we have devised new diagnostic diagrams and found that known blazars occupy a region of the $\log(S_{500\,\mu m}/S_{350\,\mu m})$ versus $\log(S_{500\,\mu m}/S_{1.4\,GHz})$ plane separated from that of sub-mm sources with radio emission powered by star formation, but shared with radio galaxies and steep-spectrum radio quasars. Using this diagnostic we have selected 12 further possible candidates that turn out to be scattered in the $(r - z)$ versus $(u - r)$ plane or in the *Wide-Field Infrared Survey Explorer* colour–colour diagram, where known blazars are concentrated in well defined strips. This suggests that the majority of them are not blazars. Based on an inspection of all the available photometric data, including unpublished VISTA

⋆ E-mail: caniego@ifca.unican.es

Kilo-degree Infrared Galaxy survey photometry and new radio observations, we found that the spectral energy distributions (SEDs) of only one out of the 12 newly selected sources are compatible with being synchrotron dominated at least up to 500 μm, i.e. with being a blazar. Another object may consist of a faint blazar nucleus inside a bright star-forming galaxy. The possibility that some blazar hosts are endowed with active star formation is supported by our analysis of the SEDs of *Planck* Early Release Compact Source Catalogue blazars detected at both 545 and 857 GHz. The estimated rest-frame synchrotron peak frequencies of H-ATLAS blazars are in the range $11.5 \leq \log(\nu_{\rm peak,\,Hz}) \leq 13.7$, implying that these objects are low synchrotron peak. Six of them also show evidence of an ultraviolet excess that can be attributed to emission from the accretion disc. Allowing for the possibility of misidentifications and of contamination of the 500 μm flux density by the dusty torus or by the host galaxy, we estimate that there are seven or eight pure synchrotron sources brighter than $S_{500\,\mu\rm m} = 35$ mJy over the studied area, a result that sets important constraints on blazar evolutionary models.

Key words: BL Lacertae objects: general – quasars: general – submillimetre: general.

1 INTRODUCTION

Blazars are a subclass of active galactic nuclei (AGN) characterized by non-thermal continuum emission from radio to γ-rays. They have extreme properties: are strongly variable across the full electromagnetic spectrum, reach very high observed luminosities and are frequently strongly polarized. Their spectral energy distribution (SED) is characterized by two broad peaks in νL_ν. The first peak occurs at a frequency $\nu_{\rm p}^{\rm s}$ varying from $\sim 10^{12}$ to $\sim 10^{19}$ Hz ($\sim$300 to $\sim 3 \times 10^{-5}$ μm; Nieppola, Tornikoski & Valtaoja 2006) and is attributed to Doppler boosted synchrotron emission from a highly relativistic jet pointing towards the observer. The continuum spectrum is 'flat' (spectral index $\alpha \gtrsim -0.5$, $S_\nu \propto \nu^\alpha$) from radio to sub-mm or even shorter wavelengths. The second peak, attributed to inverse Compton scattering, occurs at γ-ray energies.

However, the non-thermal emission not always outshines other components, like emission from the host galaxy, from the accretion disc and from the circumnuclear torus, to the point of making such components undetectable. Blazar hosts are generally found to be early-type galaxies (Kotilainen, Falomo & Scarpa 1998; O'Dowd & Urry 2005; Kotilainen et al. 2007; León-Tavares et al. 2011) and may therefore contaminate the non-thermal spectrum primarily at optical/near-infrared (IR) wavelengths. However, we should also take into account the possibility that at least some of them are endowed with star formation activity associated with thermal dust emission at far-IR/sub-mm wavelengths. The direct thermal emission from the accretion disc may show up as a relatively narrow 'bump' in the optical/ultraviolet (UV; Dermer & Schlickeiser 1993; Ghisellini & Tavecchio 2009), while the thermal emission from the dusty circumnuclear torus may be detectable in the mid-IR (Perlman et al. 2008).[1]

The optical spectra of blazars show a striking dichotomy, leading to the general recognition of two subclasses: BL Lacs with an almost featureless spectrum and flat-spectrum radio quasars (FSRQs) with strong, broad emission lines. (Padovani & Giommi 1995) classified the BL Lacs on the basis of the radio–optical, $\alpha_{\rm ro}$, and optical–X-ray, $\alpha_{\rm ox}$, spectral indices (which translate into the values of the synchrotron peak frequencies, $\nu_{\rm p}^{\rm s}$) into low-, intermediate- and high-frequency peaked. This classification was extended by (Abdo et al. 2010) to all blazars: low synchrotron peak (LSP; $\nu_{\rm p}^{\rm s} < 10^{14}$ Hz), intermediate synchrotron peak (ISP; $10^{14} < \nu_{\rm p}^{\rm s} < 10^{15}$ Hz) and high synchrotron peak (HSP; $\nu_{\rm p}^{\rm s} > 10^{15}$ Hz) objects. The distribution of $\nu_{\rm p}^{\rm s}$ is bimodal, with only a minor fraction of objects peaking at intermediate frequencies. The bimodality however may be, at least partly, due to the blazar selection which, so far, was mostly done either in the radio or in the X-ray band. The former selection favours LSPs, the latter HSPs.

The *Herschel*[2] selection, at intermediate frequencies, should help us to pick up ISPs, thus providing constraints on the abundance of these objects and indications on whether or not there is a continuity in the blazar population, from LSPs to HSPs. Moreover, a full frequency coverage is crucial to disentangle the different, non-thermal and thermal, contributions to the blazar SEDs, as briefly summarized above. The *Herschel* Astrophysical Terahertz Large Area Survey (H-ATLAS[3]; Eales et al. 2010), the largest area extragalactic survey carried out by the *Herschel* space observatory (Pilbratt et al. 2010) covering $\sim$550 deg^2 with Photodetector Array Camera and Spectrometer (PACS; Poglitsch et al. 2010) and Spectral and Photometric Imaging Receiver (SPIRE; Griffin et al. 2010) instruments between 100 and 500 μm, provides an unprecedented opportunity to obtain flux density limited blazar samples at sub-mm wavelengths. As for the non-thermal emission, the *Herschel* data cover a particularly interesting frequency range close to the $\nu_{\rm p}^{\rm s}$ of the most luminous LSPs (Fossati et al. 1998), where information is currently scanty (Padovani et al. 2006). The synchrotron peak frequency carries information on key physical parameters such as the Doppler factor of the jet, the electron energy distribution and the magnetic field strength (Dermer 1995; Massaro, Paggi & Cavaliere 2011b; Tramacere, Massaro & Taylor 2011). Moreover, the sub-mm selection is especially well suited to look for signatures of thermal dust emission from the host galaxy, thus providing a new perspective on blazar hosts and allowing us to test the early-type host paradigm.

Blazars are however a tiny fraction of H-ATLAS sources: their estimated surface density at the H-ATLAS 5σ detection limits is $\sim$0.1 per cent or less of the surface density of dusty galaxies (De Zotti et al. 2005; Tucci et al. 2011). Singling them out is not easy and appropriate diagnostic tools must be devised. An investigation

[1] It is worth noticing, however, that (Plotkin et al. 2012), using data from the *Wide-Field Infrared Survey Explorer* (*WISE*), did not see observational signatures of the dusty torus from a sample of weakly beamed BL Lac objects.

[2] *Herschel* is an ESA space observatory with science instruments provided by European-led Principal Investigator consortia and with important participation from NASA.

[3] http://www.h-atlas.org.

of the H-ATLAS science demonstration phase (SDP) field (González-Nuevo et al. 2010) uncovered two blazars brighter than the average 5σ detection limit at 500 μm, $S_{500\,\mu m} \simeq 44$ mJy (Rigby et al. 2011), over an area of 14.4 deg^2. In this paper we extend the analysis to an area almost an order of magnitude larger, as a step towards building the first statistically meaningful sample of sub-mm-selected blazars.

A key aim of this paper is to investigate the potential of this new selection band to discover blazars with unusual spectral properties. In particular, the sub-mm selection is ideal to ascertain whether some fraction of blazar host galaxies are endowed with active star formation and to assess the contribution of dusty tori at these wavelengths. The current notion that blazars are generally hosted by passive early-type galaxies is based on studies of relatively local BL Lacs. It goes along with the finding that in the local Universe the hosts galaxies of all populations of powerful radio-loud AGN do not have high star formation rates. On the other hand, it has long been known (e.g. McCarthy 1993) that radio galaxies at substantial redshifts may show intense star formation activity (an early spectacular example is 4C 41.17; Chini & Kruegel 1994; Dunlop et al. 1994). Thus, in the framework of unified models we do expect to find also blazars hosted by star-forming galaxies. Since such objects would have 'anomalous' colours we cannot expect that, in colour–colour diagrams, they lie in the same region as blazars selected at other wavelengths. This will force us to use rather loose constraints on diagnostic diagrams, at the cost of a relatively low selection efficiency.

The layout of this paper is the following. In Section 2 we describe the selection of candidate blazars, present the new diagnostic diagrams we have devised and report on the follow-up observations aimed at assessing the nature of the selected candidates. In Section 3 we briefly discuss their SEDs, built by combining the H-ATLAS photometry with literature and unpublished VISTA Kilo-degree Infrared Galaxy (VIKING) survey data. In Section 4 we discuss constraints on sub-mm blazar counts and implications for evolutionary models. Finally, Section 5 summarizes our main results.

We adopt a flat cosmology with $\Omega_\Lambda = 0.734$, $\Omega_m = 0.266$ and $h = 0.71$ as derived from the *Wilkinson Microwave Anisotropy Probe* (*WMAP*) 7-year data (Larson et al. 2011).

2 BLAZAR CANDIDATES

In this study we use the catalogue of SPIRE sources detected in the two H-ATLAS equatorial fields centred at about 9^h and 15^h, plus half of that at 12^h, with areas of 53.25, 53.93 and 27.37 deg^2, respectively, for a total of 134.55 deg^2. In the Phase 1 data release (Hoyos et al., in preparation; Valiante et al., in preparation) data for the full 12^h field will be included. The catalogue contains sources that have been detected in the noise-weighted point spread function (PSF)-filtered 250 μm map applying the MADX algorithm (Maddox et al., in preparation). Then, at the position of the sources, flux densities are estimated at each of the SPIRE bands. Finally, only sources with a signal-to-noise ratio (S/N) ≥ 5 at any of the SPIRE bands are included in the catalogue. The H-ATLAS maps and data reduction are discussed in Pascale et al. (2011) and Ibar et al. (2010), the source catalogue creation is described in Rigby et al. (2011). The SPIRE beams have full width at half-maximum (FWHM) of 18.1, 24.8 and 35.2 arcsec for 250, 350 and 500 μm, respectively (Swinyard et al. 2010; Rigby et al. 2011). The catalogue we have used contains 66 535 unique objects (26 369 in the 9^h field, 12 686 in the 12^h field and 27 480 in the 15^h field). Since blazars have red sub-mm colours (see e.g. fig. 11 of Herranz et al. 2013) they are more easily singled out at the longer wavelengths. We have therefore confined ourselves to sources with $S_{500\,\mu m} \geq 35$ mJy, corresponding to 4σ detections at this wavelength. There are 11 655 sources satisfying this criterion.

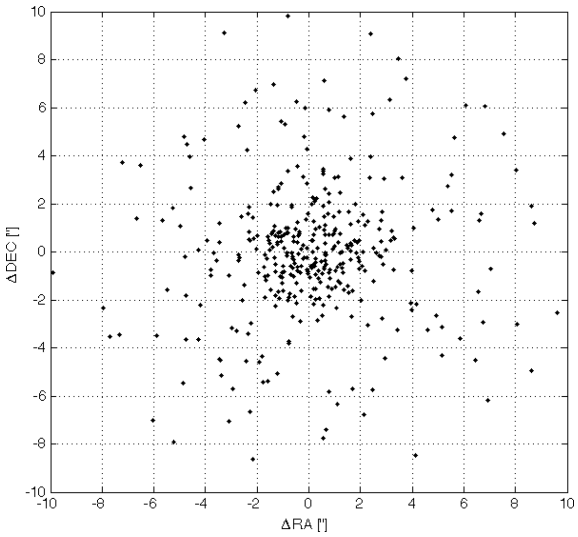

Figure 1. Positional offset between the 379 H-ATLAS sources with $S_{500\,\mu m} \geq 35$ mJy and their FIRST counterpart within 10 arcsec.

Blazars are powerful radio sources. Thus the first step towards spotting them is to require that they are detected by radio surveys covering our fields. A cross-correlation of these sources with the Faint Images of the Radio Sky at Twenty-cm (FIRST) survey catalogue (Becker, White & Helfand 1995) with a 10 arcsec search radius yields 379 matches, out of the ∼11 000 FIRST sources present in the ∼135 deg^2 H-ATLAS equatorial fields. The sample made of the 379 sources selected as described above ($S_{500\,\mu m} \geq 35$ mJy and FIRST counterpart within 10 arcsec) will be referred to as the parent sample. Almost all the objects in this sample are likely to be pure star-forming galaxies or radio galaxies in star-forming hosts as studied in (Jarvis et al. 2010) and (Hardcastle et al. 2010), respectively.

The typical rms positional error for our sources is 2.5 arcsec or less (Rigby et al. 2011),[4] and the FIRST positions are accurate to better than 0.5 arcsec for $S_{1.4\,GHz} > 3$ mJy, so that the rms offset between the radio and the sub-mm position is $\sigma \leq 2.55$ arcsec (see Fig. 1). In the case of a Gaussian distribution of positional errors the probability that a true counterpart has an apparent positional offset $\geq\Delta$ is

$$p(>\Delta) = \exp[-0.5(\Delta/\sigma)^2]. \quad (1)$$

For $\Delta = 10$ arcsec, $p(>\Delta) \leq 4.6 \times 10^{-4}$ and the number of true FIRST counterparts that we may have missed with our 11 655 trials is ≃5, i.e. ≃1.5 per cent of the parent sample.

The surface density of FIRST sources is $n_{FIRST} \simeq 90\,deg^{-2}$. Therefore the probability that a FIRST source lies by chance within $\Delta = 10$ arcsec from a given *Herschel* source is $\pi\Delta^2 n_{FIRST} \simeq 2 \times 10^{-3}$ and the expected number of chance associations is ≃25. However, as we will see in the following, from the distribution of $S_{500\,\mu m}/S_{1.4\,GHz}$ flux density ratios of known blazars we infer that genuine blazars must have $S_{500\,\mu m}/S_{1.4\,GHz} < 2.4$ or, in

[4] The quoted positional error refers to $>5\sigma$ 250 μm sources as most (355) of the 379 sources in the parent sample are.

our case, $S_{1.4\,\mathrm{GHz}} > 14$ mJy. The surface density above this limit is $\simeq$13.5 deg^{-2} and the number of chance associations decreases to $\simeq$4.

2.1 The blazar selection

Blazars are expected to be a very small fraction ($\sim$5 per cent) of the 379 sources in the parent sample. For most of them the radio emission is related to star formation, through the well-known far-IR/radio correlation (Helou, Soifer & Rowan-Robinson 1985; Condon, Anderson & Helou 1991). A first step towards picking up blazars is to restrict the sample to radio-loud objects. The distribution of sources in the $S_{500\,\mu\mathrm{m}}/S_{1.4\,\mathrm{GHz}}$ versus $S_{500\,\mu\mathrm{m}}/S_{350\,\mu\mathrm{m}}$ diagram is shown in Fig. 2.

To locate the 'blazar region' in this diagram we have looked for known blazars in the parent sample by cross-matching them with the most recent version of the blazar catalogue BZCAT (Massaro et al. 2011c), again with a search radius of 10 arcsec. We got eight matches (see Table 1). Since the BZCAT positions are mostly taken from radio catalogues and are generally better than 1 arcsec, after equation (1) the expected number of real matches that may have been missed with our 379 trials is $\leq$0.4. The probability that a BZCAT source lies by chance within 10 arcsec from a given *Herschel* source is difficult to assess accurately because of the inhomogeneous distribution of BZCAT sources. However the BZCAT catalogue contains $\simeq$3100 sources over the whole sky so that their mean surface density is $n_{\mathrm{BZCAT}} < 0.1$ deg^{-2}. If they were uniformly distributed the expected number of chance associations would be $<10^{-3}$. There is therefore a wide enough margin to confidently assume that all the associations found are real even though the distribution is not uniform. In particular, of the eight matches found with a search radius of 10 arcsec, the two with the largest angular distance to a FIRST source (objects #1 and 2 of Table 1, with a separation of 8.67 and 9.72 arcsec, respectively) have $S_{1.4\,\mathrm{GHz}} > 300$ mJy. Since the surface density of FIRST sources brighter than 300 mJy is $\sim$0.46 deg^{-2}, the probability of a chance association within 10 arcsec is $\sim 1.1 \times 10^{-5}$ and the expected number of chance associations within 10 arcsec is 0.13. On the other hand, after equation (1) the probability that a true counterpart has a positional offset of 9.72 arcsec or of 8.67 arcsec is $\simeq 7 \times 10^{-4}$ or $\simeq 3 \times 10^{-3}$, respectively. Thus the blazar classification of these two H-ATLAS sources must be taken with caution.

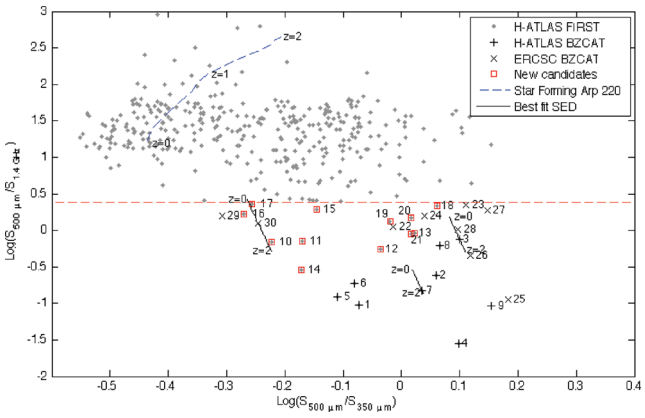

Figure 2. $S_{500\,\mu\mathrm{m}}/S_{1.4\,\mathrm{GHz}}$ versus $S_{500\,\mu\mathrm{m}}/S_{350\,\mu\mathrm{m}}$ for H-ATLAS sources with $S_{500\,\mu\mathrm{m}} \geq 35$ mJy and FIRST counterparts (parent sample). These sources are represented by the grey dots, except for the nine catalogued blazars that are identified by the larger black + signs. The grey + signs enclosed in red squares denote the radio-loud sources among which we search for new blazar candidates. Both catalogued blazars and radio-loud H-ATLAS sources are labelled with their ID numbers (see Tables 1 and 3). We also show the *Planck* ERCSC blazars detected both at 545 and at 857 GHz (see text), represented by the black × signs and labelled with the ID numbers in Table 2. The blue dashed line shows the colour–colour track, as a function of redshift, of a prototype star-forming galaxy, Arp 220, while the three black solid lines (in the lower part of the figure) show the tracks, as a function of redshift, of three blazars, assumed to have a parabolic SED, representative of the synchrotron peak. The error bars in $\log(S_{500\,\mu\mathrm{m}}/S_{1.4\,\mathrm{GHz}})$ for the catalogued and candidate blazars are $\leq$0.1 and have not been plotted for the sake of clarity.

In the BZCAT catalogue there are 15 additional blazars located in our fields. For only two of them could we detect a significant signal in the H-ATLAS noise-weighted beam convolved maps. One (BZB J0849+0206) has a 500 μm flux density of 31.6 mJy (S/N $\simeq$ 3.6) and is weaker at 250 and 350 μm (S/N $\simeq$ 2.1 and 2.2, respectively). Since this object is fainter than the adopted flux-density limit ($S_{500\,\mu\mathrm{m}} = 35$ mJy) we have not considered it further. The other object (BZQ J1404−0013) has $S_{500\,\mu\mathrm{m}} = 45$ mJy, i.e. is a 5σ detection at this wavelength, but is below the 5σ detection limit at 250 and 350 μm ($S_{250\,\mu\mathrm{m}} \simeq 18 \pm 7$ mJy and $S_{350\,\mu\mathrm{m}} \simeq 32 \pm 8$ mJy). It was probably missed because of its low 250 μm flux density (candidate sources were identified as >2.5σ peaks at 250 μm; Rigby et al. 2011); moreover, it lies close to the border of the field. We have added this source to our blazar sample. We have also searched the 2-year *Fermi*-Large Area Telescope (LAT) catalogue[5] (Ackermann et al. 2012) for sources lying in the H-ATLAS fields and not listed in the BZCAT. Only one was found, identified as a pulsar and about 3 arcmin away from the nearest source in the parent sample. Four of our objects (#1, 2, 3 and 5) were previously associated with a *Fermi*-LAT source in BZCAT.

To increase the sample of known blazars with measured sub-mm colours we have cross-correlated the full-sky *Planck* Early Release Compact Source Catalogue (ERCSC; Planck Collaboration 2011a) at 545 and 857 GHz with the BZCAT, using a search radius of 150 arcsec corresponding to the *Planck* FWHM/2 at these two bands. We also require that each *Planck* association with a BZCAT object has a flux density measurement at both *Planck* frequencies. We have listed in Table 2 the 14 matches that fulfil these requirements. Five of these sources, however, were excluded from further analysis because an inspection of the NASA Extragalactic Database[6] (NED) shows that BZU J1325−4301 is the well-known extended radio galaxy Centaurus A for which it is difficult to single out the nuclear emission; the blazar classification of BZB J1136+1601 is dubious; BZU J2209−4710 (alias NGC 7213) has sub-mm colours typical of thermal dust emission from the host galaxy and the ERCSC flux densities of BZQ J1559+0304 and BZQ J1719+0817 may be affected by source blending. We are then left with nine blazars (objects #22–30 in Table 2), whose colours are also plotted in Fig. 2 .

According to the technical specifications of their respective instruments, the *Planck*/High Frequency Instrument (HFI) 857 GHz and the *Herschel*/SPIRE 350 μm channels have almost exactly the same central wavelength and roughly the same bandwidth. The comparison between the *Planck* 545 GHz and the SPIRE 500 μm flux densities requires a colour correction because the

[5] fermi.gsfc.nasa.gov/ssc/data/access/lat/2yr_catalog/
[6] ned.ipac.caltech.edu/

Table 1. BZCAT blazars found in the H-ATLAS 9^h, 12^h and 15^h fields. Objects BZB J0909+0200 and BZQ J0909+0121 are those found by González-Nuevo et al. (2010) in the H-ATLAS Science Demonstration Phase field. Objects #1–8 are listed in H-ATLAS catalogues while object #9 lies near a border of the map and was excluded when making the catalogues. The distance between the H-ATLAS source and the FIRST low radio frequency counterpart is shown. The redshifts are from the BZCAT.

ID	H-ATLAS IAU ID	RA (°)	Dec. (°)	$S_{250\,\mu m}$ (mJy)	$S_{350\,\mu m}$ (mJy)	$S_{500\,\mu m}$ (mJy)	S_{FIRST} (mJy)	Distance (arcsec)	z	BZCAT name	*Fermi* 2FGL name
1	HATLAS J083949.3+010436	129.95576	1.07669	50.50	50.68	42.83	443.71	9.72	1.123	BZQ J0839+0104	2FGL J0839.6+0059
2	HATLAS J090940.3+020000	137.41804	2.00013	40.29	64.49	73.87	305.76	8.67	–	BZB J0909+0200	2FGL J0909.6+0158
3	HATLAS J090910.1+012135	137.29245	1.35986	258.11	337.74	424.86	559.64	1.42	1.024	BZQ J0909+0121	2FGL J0909.1+0121
4	HATLAS J115043.8−002355	177.68276	−0.39885	37.90	63.28	79.22	2803.17	1.90	1.976	BZQ J1150−0023	
5	HATLAS J113245.7+003427	173.19054	0.57434	65.81	73.66	57.25	468.98	1.43	–	BZB J1132+0034	2FGL J1132.9+0033
6	HATLAS J113302.9+001545	173.26229	0.26256	59.41	48.56	40.35	214.96	3.99	1.173	BZQ J1133+0015	
7	HATLAS J113320.1+004054	173.33408	0.68185	35.61	43.24	46.90	312.49	2.40	1.633	BZQ J1133+0040	
8	HATLAS J141004.6+020306	212.51958	2.05174	114.23	152.90	178.05	291.62	0.80	–	BZBJ1410+0203	
9	HATLAS J140412.1−001325	211.05040	−0.22360	18.00	32.00	45.00	516.32	0.08	1.217	BZQ J1404−0013	

Table 2. BZCAT blazars with a *Planck*-ERCSC counterpart at both 545 and 857 GHz (see text). The 600 GHz flux densities were computed interpolating between measurements at 545 and 857 GHz. The redshifts are from BZCAT. Note that there are far more *Planck*-ERCSC blazars with counterparts in the 2-year *Fermi*-LAT catalogue (Giommi et al. 2012). Here we list only those detected at both 545 and 857 GHz. Objects #31–35 have been excluded from the analysis for the reasons mentioned in the text.

ID	RA (°)	Dec. (°)	$S_{545\,GHz}$ (mJy)	$S_{600\,GHz}$ (mJy)	$S_{857\,GHz}$ (mJy)	$S_{1.4\,GHz}$ (mJy)	z	BZCAT name	2FGL name
22	140.2420	44.6956	1142.91	1152.93	1190.84	1017.00	2.190	BZQ J0920+4441	2FGL J0920.9+4441
23	133.7000	20.1131	3618.51	3377.79	2616.81	1512.00	0.306	BZB J0854+2006	
24	343.4920	16.1481	20 585.74	20 086.98	18 340.72	12 657.00	0.859	BZQ J2253+1608	
25	187.2750	2.0458	6937.50	6193.01	4065.28	54 991.00	0.158	BZQ J1229+0203	
26	194.0420	−5.7894	4701.58	4370.46	3333.65	9711.00	0.536	BZQ J1256−0547	
27	60.9710	−36.0869	2338.46	2134.30	1521.04	1151.00	1.417	BZQ J0403−3605	
28	84.7120	−44.0853	4065.40	3826.54	3057.01	3729.00	0.892	BZB J0538−4405	
29	140.3960	62.2628	1234.73	1495.28	3041.21	946.00	1.446	BZQ J0921+6215	
30	130.1979	13.2066	2801.51	3263.22	5745.42	2614.00	0.681	BZU J0840+1312	2FGL J0840.7+1310
31	239.8787	3.0801	2852.39	3628.80	8860.86	400.00	3.891	BZQ J1559+0304	
32	259.9675	8.2843	2335.54	2786.30	5361.02	313.00	1.185	BZQ J1719+0817	
33	332.3175	−47.1667	1113.74	1451.80	3879.44	98.00	0.006	BZU J2209−4710	
34	201.3650	−43.0191	42 536.85	52 573.14	11 5319.12	5700.00	0.002	BZU J1325−4301	2FGL J1325.6−4300
35	174.0725	16.0314	2231.71	2685.59	5335.52	17.00	0.574	BZB J1136+1601	

central frequency of the 500 μm channel is somewhat higher (≃600 GHz). The extrapolation from 545 to 600 GHz was made using, for each *Planck* blazar, its spectral index between 545 and 857 GHz; since the spectral indices are quite flat, the corrections are small.

Fig. 2 shows that the nine known blazars in our H-ATLAS fields and the nine ERCSC blazars lie in a region in the $\log(S_{500\,\mu m}/S_{1.4\,GHz})$ versus $\log(S_{500\,\mu m}/S_{350\,\mu m})$ plane fairly well separated from the region populated by the majority of the other sources in our parent sample that have a $S_{500\,\mu m}/S_{1.4\,GHz} \geq 10$, typical of star-forming galaxies. To illustrate this further, we have included in this panel a blue dashed line that represents the colour track as a function of redshift of the prototype starburst galaxy Arp 220. Our choice of the boundary line between star formation and AGN powered radio emission is consistent with the value of $\langle \log S_{250\,\mu m}/S_{1.4\,GHz} \rangle - 3\sigma$ found by Ivison et al. (2010) for star-forming galaxies, after allowing for a typical ratio $S_{250\,\mu m}/S_{500\,\mu m} \simeq 2$ (at a typical $z \simeq 1$).

The $S_{500\,\mu m}/S_{1.4\,GHz}$ ratios of blazars are $\lesssim$2.4 and their $S_{500\,\mu m}/S_{350\,\mu m}$ colours are redder than average. This upper limit to the $S_{500\,\mu m}/S_{1.4\,GHz}$ ratio for blazars comes from the ERCSC objects, while the H-ATLAS ones, which may be thought to be more relevant here, have significantly lower ratios. But we must beware of a selection effect. Since the BZCAT blazars are mostly radio selected (with important additions from X-ray and γ-ray selections), relatively radio-faint objects, such as possible H-ATLAS blazars with high $S_{500\,\mu m}/S_{1.4\,GHz}$ ratios, are easily missed by previous blazar searches. The situation is different for the much (generally more than 10 times) brighter ERCSC blazars for which we likely have the full range of $S_{500\,\mu m}/S_{1.4\,GHz}$ ratios. We have therefore adopted

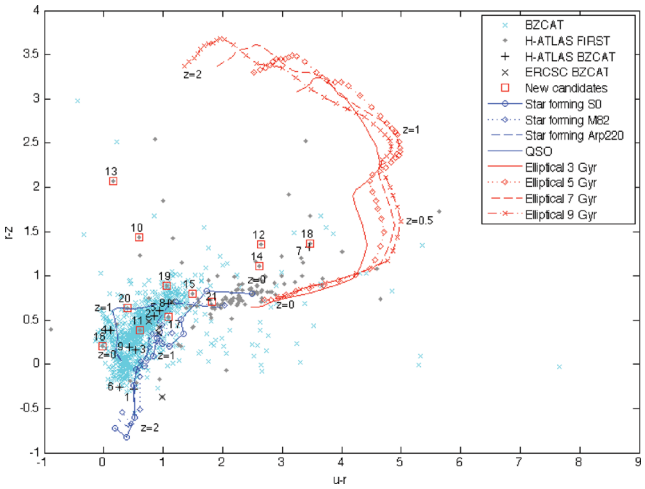

Figure 3. Diagnostic colour–colour diagram: $(r - z)$ versus $(u - r)$ (lower panel). The grey dots, the black + signs and grey + signs enclosed in red squares have the same meaning as in Fig. 2. Only a subset of sources in the parent sample has SDSS photometry and thus appears also in this figure. The cyan × signs correspond to BZCAT blazars with SDSS photometry. We also show, for comparison, the colour–colour tracks, as a function of redshift, of four passive elliptical templates of different ages (red lines) and of three star-forming galaxies (blue lines). The S0, M82, QSO and Arp 220 tracks were computed using the SEDs tabulated in the SWIRE library (Polletta et al. 2007) available at http://www.iasf-milano.inaf.it/~polletta/templates/swire_templates.html. The elliptical galaxy tracks were computed using GALSYTH, the web based interface for the GRASIL model (Silva et al. 1998) available at http://galsynth.oapd.inaf.it/galsynth/. The colours corresponding to some redshift values are indicated. The typical errors in $(r - z)$ and $(u - r)$ are 0.046 and 0.091, respectively.

as the limiting ratio, the maximum value for ERCSC blazars, shown with a dashed red line in Fig. 2.

On the whole, ERCSC blazars greatly extend the 'blazar region' in the $S_{500\,\mu m}/S_{1.4\,GHz}$ versus $S_{500\,\mu m}/S_{350\,\mu m}$ diagram compared to that populated by known H-ATLAS blazars. On one side, this highlights the power of the sub-mm selection in finding blazars with 'anomalous' properties. On the other side, a broader blazar region is more easily contaminated by other source populations, implying a lower efficiency in the selection of true blazars; this is however the usual price to be paid by exploratory studies aiming at opening new perspectives. The black solid lines in Fig. 2, showing the colour tracks as a function of redshift for three objects in our sample assuming a parabolic SED, representative of blazars, confirm that these sources indeed populate the part of the diagram with $S_{500\,\mu m}/S_{1.4\,GHz} < 10$. However, since we are using low-frequency (1.4 GHz) radio observations, is expected that most objects below the dashed boundary line are steep-spectrum radio galaxies or quasars. We then need to find diagnostic tools capable of singling out good blazar candidates.

To this end we have built the $(r - z)$ versus $(u - r)$ colour–colour diagram (Fig. 3) for known blazars by cross-correlating the SDSS Data Release 8 (DR8)[7] catalogue (Aihara et al. 2011) with the BZCAT, using a search radius of 0.5 arcsec. The surface density of DR8 sources is $\simeq 3.22 \times 10^4$ deg^{-2} so that the probability of a chance association within 0.5 arcsec is $\simeq 2 \times 10^{-3}$. Since there are $\simeq$1800 BZCAT sources within the DR8 area, we expect $\simeq$3.5 chance associations. We get 1600 matches. They are mostly concentrated along a relatively narrow strip in the $(r - z)$ versus $(u - r)$ plane. As illustrated by the colour tracks in Fig. 3, the blazar region is bounded on the right by the region occupied by galaxies with intense star formation activity and on the left by the region of optical quasi-stellar objects (QSOs), while passive early-type galaxies are much redder in both colours. Thus very red colours are indicative of contamination by a passive early-type host galaxy. Indications that $(u - r) > 1.4$ likely implies host galaxy contamination were previously reported by Massaro, Nesci & Piranomonte (2012).

Seven out of the 12 radio-loud objects (#11, 15, 16, 17, 19, 20 and 21) lie within or very close to the blazar strip in the $(r - z)$ versus $(u - r)$ diagram, although the *Herschel*/SPIRE colours of #16 and 17 are indicative of contamination by dust emission in the host galaxy. Objects #12, 14 and 18 are at, or somewhat above, the red end of the strip, suggesting that their optical colours may be contaminated by the stellar component of the host galaxy. Hints of additional contamination from the host galaxy dust emission come from the *Herschel*/SPIRE colours of two of these objects (#12 and 14). The sub-mm to optical photometric data on one of the two outliers with blue $(u - r)$ colours (object #10) are strongly indicative of a star-forming galaxy. The other blue outlier (object #13) is anomalously faint in the r band (compared to neighbour bands); its $(r - z)$ versus $(u - r)$ colours may thus not be a good diagnostic. Some of our radio-loud objects have optical colours consistent with those of QSOs.

Another diagnostic tool, based on the [3.4][4.6][12] μm colour–colour diagram using *WISE* (Wright et al. 2010) magnitudes, was proposed by Massaro et al. (2011a). Magnitudes for the three *WISE* channels are available[8] for 7 H-ATLAS catalogued blazars (the exceptions are #7 and 9) and for nine of our radio-loud objects (the exceptions are #11, 14 and 15). The cross-match was performed using the *WISE* All-Sky Source Catalog multi-object search tool, with a search radius of 5 arcsec. All the 16 associations found are unique, i.e. there were no multiple matches. The positions of H-ATLAS catalogued blazars and radio-loud sources are identified, in Fig. 4, by their ID numbers (see Tables 1 and 3). The catalogued H-ATLAS blazars for which *WISE* photometry is available plus the radio-loud sources #10, 16 and 20 lie in the upper part of 'blazar strip', i.e. in the region occupied by flat-spectrum radio quasars (although #16 is at the border). Four of our radio-loud sources (#12, 13, 18 and 21) have *WISE* colours typical of starburst galaxies, and two (#17 and 19) are in the regions populated by low-ionization nuclear emission-line regions (LINERs)/obscured AGN or ultraluminous infrared galaxies (ULIRGs).[9]

Other indications on the nature of our radio-loud sources can be obtained from the radio morphology. To investigate it we have extracted images centred at their position using the FIRST image cut-out tool. Seven sources (#12, 13, 14, 16, 17, 19 and 20) look point like, three (#11, 15 and 21) show a core-jet morphology with a dominant core, while the other two (#10 and 18) are clearly double with similarly bright blobs, consistent with them being steep-spectrum radio galaxies or quasars. Three of the candidates (#10, 15 and 18) have 1.4 GHz NRAO VLA Sky Survey (NVSS) flux densities larger than the FIRST ones by a factor of >2. Since FIRST has a much higher angular resolution than NVSS, this is consistent with these sources being extended.

[7] www.sdss3.org/dr8/

[8] irsa.ipac.caltech.edu/Missions/wise.html

[9] wise2.ipac.caltech.edu/docs/release/prelim/expsup/figures/sec2_2f16_annot.gif

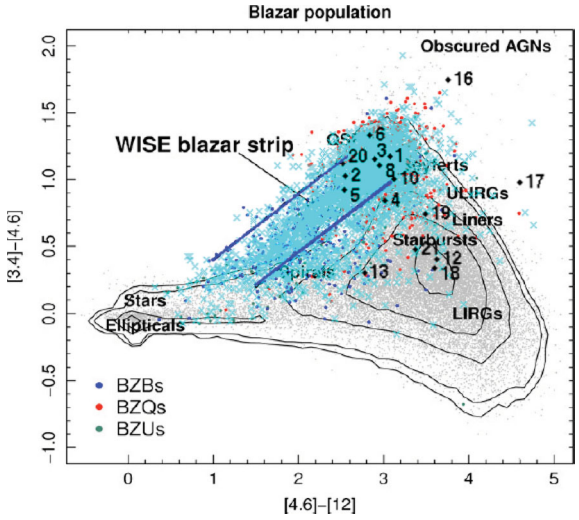

Figure 4. Diagnostic diagram using *WISE* colours. BZCAT objects are shown in cyan and our radio-loud sources and the catalogued blazars are labelled with their ID numbers (see Tables 1 and 3). The other data points and the boundaries of the '*WISE* blazar strip' are from (Massaro et al. 2011a). BZB, BZQ and BZU stand for BL Lac, flat-spectrum radio quasar and blazar of uncertain type, respectively. The contours tracing the density of sources in colour bins with annotations showing the location of different classes of objects are from the *WISE* Explanatory Supplement (Cutri et al. 2011).

2.2 Follow-up radio observations

We have performed follow-up observations with the Medicina 32-m single-dish telescope at 5 GHz of six of our radio-loud sources. Observations were carried out between 2011 August 1 and 16 in the OTF scan mode (Mangum, Emerson & Greisen 2007; Righini 2008) applying the observing strategy, the data reduction procedures and the software tools developed for the SiMPlE project (Procopio et al. 2011). 25^{h} were allocated for 5 GHz observations with a single feed receiver and a 150-MHz-wide band. The 37 arcmin length of each scan ($\sim$5 $\times$ HPBW) was covered at 3 arcmin s^{-1} in 12.5 s. A sampling rate of 40 ms allowed us to obtain 60 samples beam^{-1}. The scans were centred on the FIRST positions.

Given the FIRST flux densities we do not expect to see any of our targets in a single scan, which, in optimal observing conditions, should hence appear as a linear baseline that corresponds to the off-source zero level of the signal. Along the scans, Gaussian noise shows up as amplitude fluctuations. However, cloudy weather, the presence of random, but unfortunately not rare, contributions by radio frequency interference (RFI) or digital noise heavily affected portions of the data. These disturbances give rise to bumpy baselines or spike-like features. All the scans that do not show a linear profile or show such features were removed before running the data reduction pipeline.

We have used the OTF Scan Calibration–Reduction (OSCAR) pipeline (Procopio et al. 2011; Righini, in preparation) to get the conversion factor from raw data counts measured on calibrators to their known flux densities, to determine the component of the flux density error due to calibration and to calculate the source flux densities and their errors. 3C 295 and 3C 286 were used as flux density calibrators. One out of the six targeted sources was not detected because of technical problems. The 5 GHz flux densities for the other five sources were measured with S/N greater than 6. The results are given in Table 4. Source #14 turned out to have a steep 1.4–5 GHz spectral index and is optically identified as a galaxy. For the other four sources (#10, 11, 13 and 21) our observations indicate a flat spectral index, consistent with them being blazars. We caution, however, that the low-frequency spectral index is not necessarily a conclusive indication for or against a blazar classification since the low-frequency radio emission frequently comes from a different component. Additional flux density measurements up to mm wavelengths are necessary to assess the nature of candidate blazars. Such observations have been planned, and preliminary results for some of the candidates are available.

Table 4. Flux densities (mJy) at 5 GHz and their errors (σ_S) measured with the Medicina radio telescope for five radio-loud sources. The FIRST 1.4 GHz flux densities (mJy) are also shown, for comparison.

ID	RA (°)	Dec. (°)	$S_{1.4\,\mathrm{GHz}}$	$S_{5\,\mathrm{GHz}}$	σ_S
10	218.522	−0.385	59.92	43.03	5.25
11	220.332	0.420	57.32	38.72	3.19
13	222.376	2.610	50.09	46.93	4.30
14	174.092	0.815	151.74	37.21	3.93
21	222.406	0.693	51.93	55.20	9.09

Table 3. New blazar candidates found in the H-ATLAS 9^{h}, 12^{h} and 15^{h} fields. Redshifts are not available for any of these objects.

ID	H-ATLAS IAU ID	RA (°)	Dec. (°)	$S_{250\,\mu m}$ (mJy)	$S_{350\,\mu m}$ (mJy)	$S_{500\,\mu m}$ (mJy)	S_{FIRST} (mJy)	Distance (arcsec)	FIRST ID	FIRST RA (^{h} ^{m} ^{s})	FIRST Dec. (° ′ ″)
10	HATLAS J143405.2−002307	218.52182	−0.38549	73.40	70.02	41.95	59.92	3.01	J143405.2−002310	14 34 05.248	−00 23 10.76
11	HATLAS J144119.7+002511	220.33240	0.41993	52.44	60.79	41.15	57.32	7.31	J144119.4+002506	14 41 19.412	+00 25 06.88
12	HATLAS J140931.9−010054	212.38320	−1.01520	43.92	38.33	35.31	63.61	7.60	J140931.4−010053	14 09 31.465	−01 00 53.83
13	HATLAS J144930.2+023636	222.37620	2.61022	24.43	43.89	46.27	50.09	4.32	J144930.3+023632	14 49 30.310	+02 36 32.48
14	HATLAS J113622.0+004854	174.09173	0.81505	99.44	65.30	43.97	151.74	2.40	J113622.0+004851	11 36 22.041	+00 48 51.80
15	HATLAS J085418.9−003612	133.57879	−0.60352	56.07	68.31	48.88	25.43	7.24	J085418.6−003619	08 54 18.690	−00 36 19.14
16	HATLAS J114616.8−001937	176.57016	−0.32712	95.44	69.55	37.28	22.17	1.11	J114616.8−001936	11 46 16.820	−00 19 36.53
17	HATLAS J114203.3+005133	175.51381	0.85938	147.77	66.52	36.79	15.92	3.00	J114203.4+005136	11 42 03.440	+00 51 36.05
18	HATLAS J142631.1+014226	216.62988	1.70600	30.70	43.20	49.80	23.39	5.92	J142631.4+014231	14 26 31.400	+01 42 31.25
19	HATLAS J143743.4−005237	219.43098	−0.87711	53.80	49.90	47.70	35.40	8.76	J143742.8−005240	14 37 42.880	−00 52 40.64
20	HATLAS J145146.2+010610	222.94281	1.10293	35.60	60.30	62.70	41.78	9.83	J145145.9+010619	14 51 45.950	+01 06 19.10
21	HATLAS J144937.4+004135	222.40611	0.69322	53.42	44.550	46.26	51.93	8.19	J144937.9+004131	14 49 37.946	+00 41 31.66

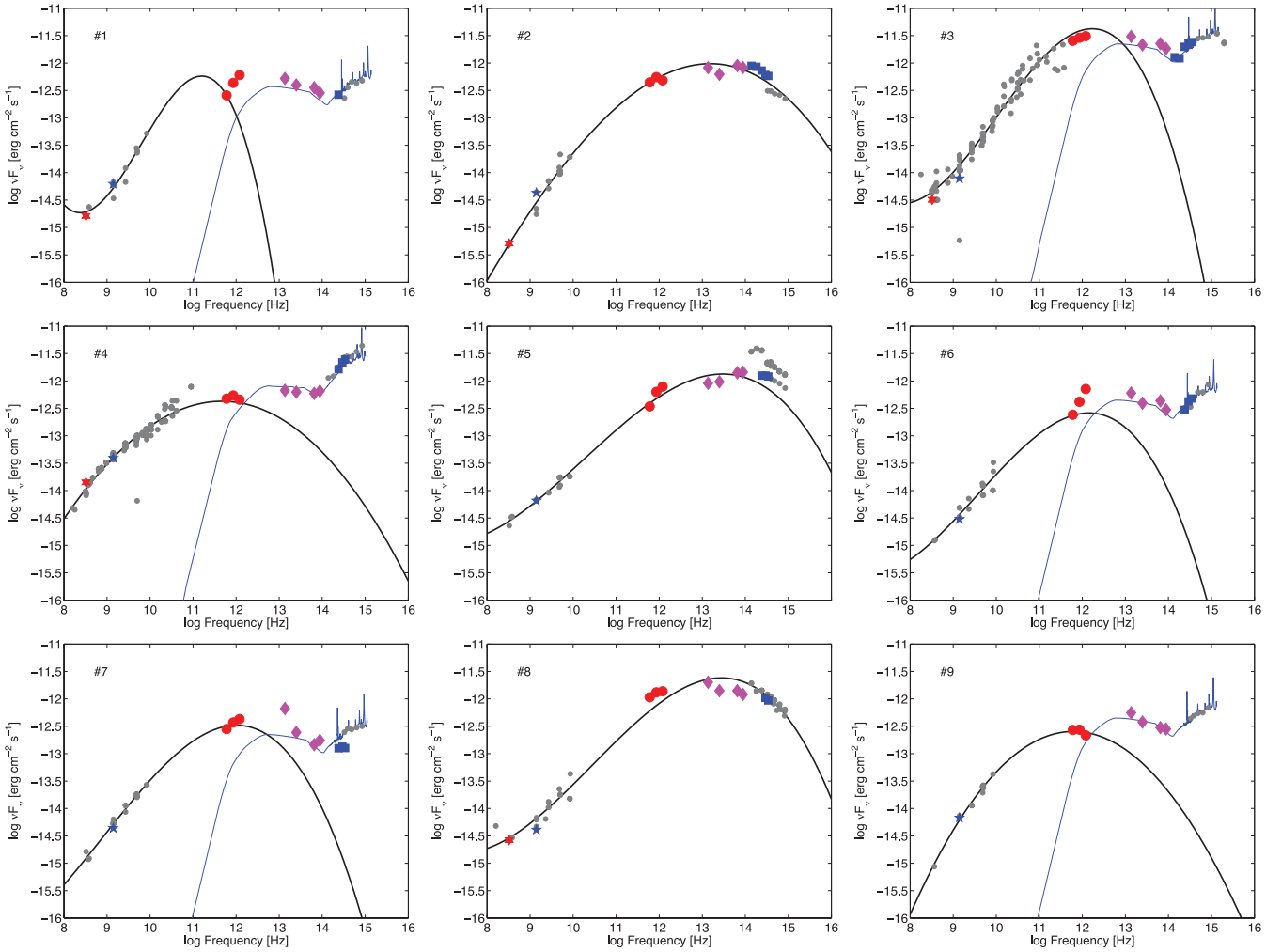

Figure 5. SEDs of the nine catalogued blazars in the H-ATLAS equatorial fields (Table 1). The red six-pointed stars, the blue five-pointed stars, the red circles, the magenta diamonds and the blue squares are GMRT, FIRST, H-ATLAS, *WISE* and VIKING survey data, respectively. The other data points are from the NED and are generally from the SDSS. The thick solid lines are second-order polynomials representing the synchrotron emission. In panels 1, 3, 4, 6 and 9 the thin blue solid lines show the type 1 QSO SEDs by Polletta et al. (2007); they are average SEDs (QSO1) except for panel 4 where the BQSO1 SED (appropriate for QSOs with particularly low-IR/optical ratios) is plotted. This template is only shown for illustration purposes and no fit to the data has been attempted: since the synchrotron component is highly variable and the data are not simultaneous, fits would have little meaning.

3 SPECTRAL ENERGY DISTRIBUTIONS

3.1 Catalogued blazars

Four out of the nine known blazars in the H-ATLAS fields have counterparts in the 2-year *Fermi*-LAT catalogue (Ackermann et al. 2012, see Table 1). The blazar J090910.1+012135 (#3) happened to be observed twice by *Herschel*, on 2009 November 22 and 2010 May 30, and showed a strong variability, thus providing a direct confirmation of the non-thermal, jet-related nature of its sub-mm emission. Its 250, 350 and 500 μm flux densities increased from 160, 194 and 266 mJy, respectively, at the first epoch, to 258, 338 and 425 mJy at the second epoch. This source was also found to be variable also in γ-rays: its *Fermi*-LAT variability index is 159.5.

Fig. 5 shows the SEDs from radio to UV frequencies of the nine known blazars in the H-ATLAS equatorial fields. To the data from the NED and to the H-ATLAS data we have added the near-IR photometry provided by the VIKING survey (Fleuren et al. 2012; Sutherland et al., in preparation) and by the *WISE* survey (Wright et al. 2010). In addition, five of our catalogued blazars and nine of our blazar candidates were detected by the Giant Metrewave Radio Telescope (GMRT) survey of H-ATLAS equatorial fields at 325 MHz (Mauch et al., in preparation). The measured flux densities are given in Table 5 and shown in Figs 5 and 6. The 0.325–1.4 GHz (FIRST) spectral indices of four catalogued blazars

Table 5. Flux densities at 325 MHz and their errors obtained with the GMRT for five confirmed blazar and nine new candidates.

ID	$S_{325\,\mathrm{MHz}}$ (mJy)	ID	$S_{325\,\mathrm{MHz}}$ (mJy)
1	500 ± 15	12	255 ± 13
2	157 ± 5	15	155 ± 5
3	986 ± 31	16	156 ± 6
4	4354 ± 124	17	72 ± 5
8	815 ± 26	18	210 ± 7
10	602 ± 21	19	84 ± 15
11	283 ± 9	21	127 ± 12

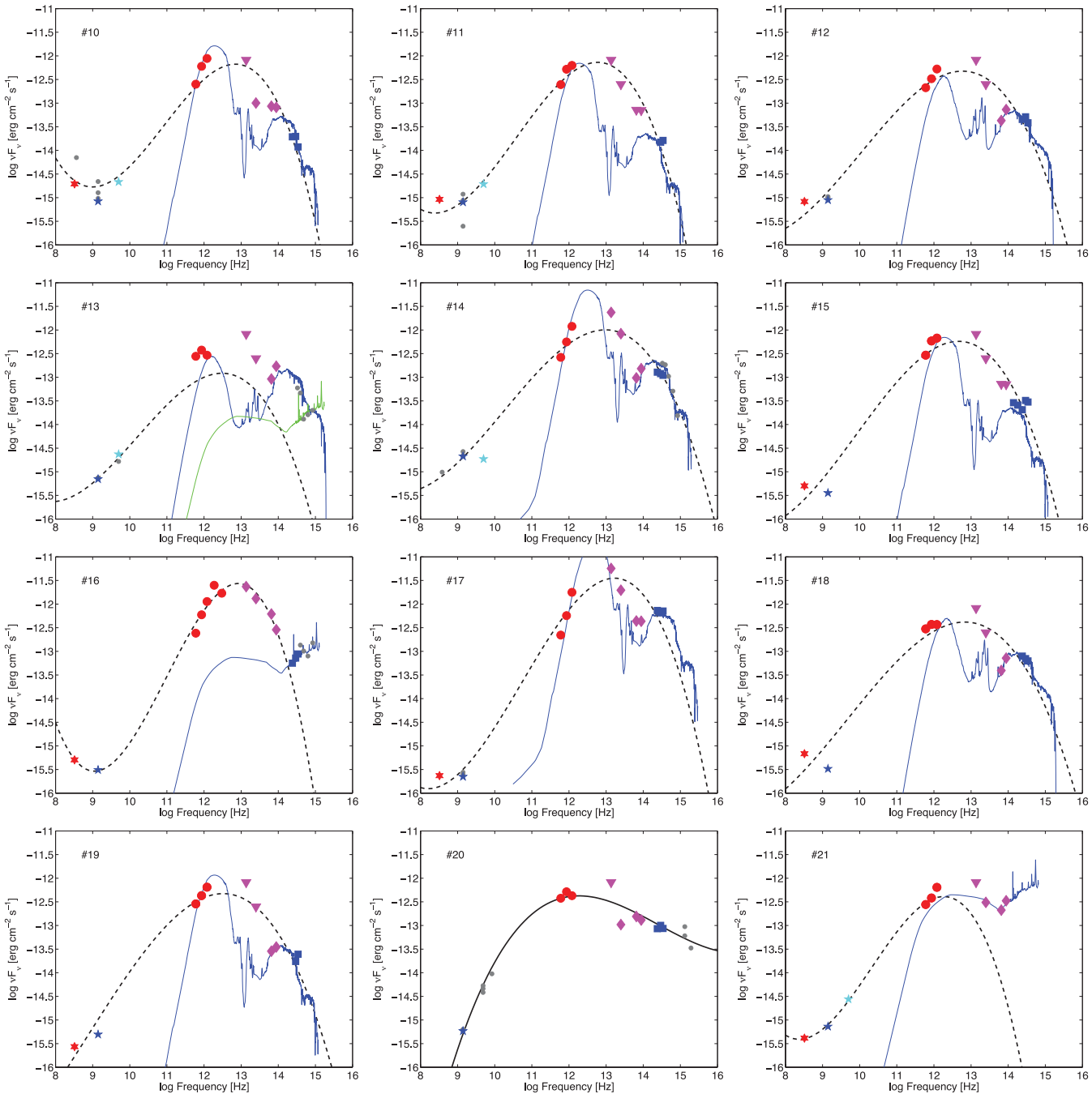

Figure 6. SEDs of the 12 radio-loud sources in the H-ATLAS equatorial fields (Table 3). The meaning of data points is the same as in Fig. 5 except that the cyan five-pointed stars at 5 GHz, shown for sources in Table 4, show the Medicina measurements and the downwards-pointing magenta triangles represent *WISE* upper limits. The black solid line, shown only for source #20, is a second-order polynomial representing the synchrotron emission. The black dashed lines shown in the other panels are again second-order polynomials and are plotted only to illustrate that a blazar-like SED cannot match the data, except for the puzzling source #16 and for the source #21, discussed in the text. The green line (in the panel referring to object #13) shows the QSO1 template by Polletta et al. (2007), that may account for the UV data. This supports the possibility that this object contains a faint blazar nucleus. The blue solid lines show the Arp 220 template from Polletta et al. (2007) for objects #10, 11, 14, 15, 17 and 19; a dusty galaxy template with $\log(L_{\rm dust}/{\rm L}_{\odot}) > 11.5$ for objects #12 and 18, and with $\log(L_{\rm dust}/{\rm L}_{\odot})$ in the range 11.0–11.5 for object #13 (Smith et al. 2012); the QSO1 SED by Polletta et al. (2007) for objects #16 and 21. As for Fig. 5, these templates are shown for illustration only: no fit of the data was attempted.

are flat or inverted ($\alpha_{0.325}^{1.4} > -0.5$, $S_\nu \propto \nu^\alpha$) while all the nine radio-loud sources (possible blazar candidates) have $\alpha_{0.325}^{1.4} < -0.5$. As noted in Section 2.2, however, a steep low-frequency spectrum is an indication, but not necessarily a proof, that the object is not a blazar since the low-frequency emission may come from a component different from the relativistic jet. In addition, all these data are far from simultaneous. Hence any fit should be dealt with great caution and can only be considered as purely indicative.

As usual (e.g. Fossati et al. 1998), we fit the synchrotron peak with a second-order polynomial (i.e. a parabola). As shown by Table 1,

six out of the nine catalogued blazars have redshift measurements. For the other three we assumed a redshift of 1.2, the median value of the 6. The estimated rest-frame synchrotron peak frequencies (in terms of νL_ν) are in the range $11.5 \leq \log(\nu_{\rm peak,\,Hz}) \leq 13.7$, with a median $\log \nu_{\rm peak,\,median,\,Hz} \simeq 12.5$. These objects are thus LSPs. In only one case (#3; see González-Nuevo et al. 2010) we have enough high-energy data to allow a meaningful estimate of the shape of the inverse Compton peak (not shown in the corresponding panel of Fig. 5). For this object, the Compton dominance, defined as the ratio between the inverse Compton and synchrotron peak luminosities is $\nu_{\rm p,\,IC} L\nu_{\rm p,\,IC} / \nu_{\rm p,\,S} L\nu_{\rm p,\,S} \simeq 8.6$. Although three other blazars have γ-ray measurements, they are missing X-ray data and therefore the rising part of the inverse Compton peak is essentially unconstrained.

Most of these blazars (#1, 3, 4, 6, 7, 9) also show evidence of a UV excess that can be attributed to emission from the accretion disc (Dermer & Schlickeiser 1993; Ghisellini & Tavecchio 2009). Under the standard assumption that the accretion disc emission is a combination of blackbodies with temperatures depending on the distance from the central black hole (equation 1 of Ghisellini & Tavecchio 2009) the black hole mass, $M_{\rm bh}$, can be estimated as

$$\frac{M_{\rm bh}}{10^9\,{\rm M}_\odot} \simeq 1.2 \left(\frac{\eta}{0.1}\right)^{-(1/2)} \left(\frac{T}{2\times10^4\,{\rm K}}\right)^{-2} \times \left(\frac{L_{\rm d}}{10^{45}\,{\rm erg\,s^{-1}}}\right)^{-(1/2)}, \quad (2)$$

where η is the mass to light conversion efficiency, T is the maximum blackbody temperature and $L_{\rm d}$ is the total luminosity of the accretion disc. The lack of sufficient simultaneous data hampers reliable estimates of the key quantities T and $L_{\rm d}$, hence of $M_{\rm bh}$. In this situation the calculation of corrections for attenuation by the intergalactic medium along the line of sight (Haardt & Madau 2012) is not warranted. Tentative values, obtained simply interpreting the UV data points, uncorrected for attenuation, as lower limits, are in the ranges $M_{\rm bh} = 0.3$–$1 \times 10^9\,{\rm M}_\odot$, with a median value of $0.7 \times 10^9\,{\rm M}_\odot$. The median accretion rate $\dot{M}_{\rm bh} = L_{\rm d}/(\eta c^2)$ is $\simeq 4\,{\rm M}_\odot\,{\rm yr}^{-1}$.

A standard type 1 QSO SED (Polletta et al. 2007) implies that the *WISE* flux densities and a fraction of sub-mm *Herschel*/SPIRE flux densities (especially at the shorter wavelengths) of our blazars with UV excess can be attributed to the dusty torus around the black hole. No contribution from the host galaxy is required for any of the nine catalogued blazars.

To complement this analysis we have considered again the catalogued blazars with counterparts in the *Planck* ERCSC at both 545 and 857 GHz (see Section 2.1), excluding only BZU J1325−4301, i.e. Centaurus A, because of the difficulty of removing the contribution of the extended emission and BZB J1136+1601 because its classification as a blazar is dubious. Thus we have now 12 ERCSC blazars. For five (i.e. ≃40 per cent) of them (BZU J0840+1312, BZQ J0921+6215, BZQ J1559+0304, BZQ J1719+0817 and BZU J2209−4710) the sub-mm continuum appears to be dominated by thermal dust emission powered by star formation. Three of these *Planck* ERCSC objects (those labelled BZQ) and both H-ATLAS blazars with possibly/likely star-forming hosts are classified in BZCAT as flat-spectrum radio quasars. This is not implausible since the far-IR luminosity of an ongoing starburst can easily outshine, around its peak wavelength, the quasar emission (e.g. Netzer et al. 2007). The starburst dominance is facilitated by the fact that the quasar bolometric luminosity is distributed over a broad wavelength range while the thermal dust emission is peaked.

3.2 Radio-loud sources

As discussed in Section 2.1, the distribution of our radio-loud sources in the diagnostic diagrams does not allow an unambiguous selection of reliable blazar candidates, while suggesting that most of these objects are steep-spectrum radio galaxies or quasars whose far-IR/sub-mm emission is dominated by the contribution of a dusty star-forming host galaxy. Clearer indications can hopefully be obtained by considering all the photometric data together, i.e. investigating the SEDs.

As shown by Fig. 6, the SEDs of most (eight out of 12) radio-loud objects (#10, 11, 12, 14, 15, 17, 18, 19) are indeed more consistent, in the sub-mm to optical range, with those of dusty galaxies, while the radio data indicate that they are probably steep spectrum. Thus these objects are not plausible blazar candidates. The SED of #13 is a bit puzzling. On one side its radio spectrum is flat but, on the other side, higher frequency data are indicative of a star-forming galaxy. Thus this source may consist of a weak blazar nucleus at the centre of a bright star-forming galaxy. Another puzzling case is object #16. Its low-frequency radio spectrum is steep while higher frequency data configure an SED consistent with a parabolic shape and markedly different from any galaxy and QSO SED. Also consistent with a parabolic shape is the SED of #20 while that of #21 can be fitted with a parabola plus a type-1 QSO SED.

Objects #13, 16 and 20 are point like in FIRST images, while #21 has a core-jet morphology, with a dominant core. These morphologies are consistent with these objects being blazars. However, preliminary results from a multifrequency follow-up observation campaign with the Australia Compact Array (Massardi et al., in preparation) show that both sources #16 and #21 have a steep radio spectrum at least up to ≃40 GHz, while object #20 is flat spectrum. So only the latter is a reliable blazar candidate. Variability and polarization measurements can provide further tests of their blazar nature.

4 NUMBER COUNTS

From the previous analysis we can conclude that of the nine BZCAT blazars with $S_{500\,\mu{\rm m}} \geq 35$ mJy over the area of 134.55 deg^2, two (#1 and 6) seem to have a substantial thermal contribution (likely from the dusty torus) to the measured 500 μm flux density. Since their flux density is close to our threshold, the pure synchrotron component is probably below that limit. It may also be noted that the radio source associated with object #1 has a relatively large angular distance from the H-ATLAS position (9.7 arcsec) and therefore may be a misidentification.

In addition we have found one valid blazar candidate (#20). We caution, however, about the possibility that the radio source is not the correct counterpart of the H-ATLAS source, given the relatively large angular separation between their positions (9.8 arcsec). Another object (#13) may consist of a faint blazar nucleus inside a bright star-forming galaxy at a measured redshift $z = 0.6995$, a configuration similar to that of the catalogued *Planck*-ERCSC blazar BZU J2209−4710.

All in all, we estimate that there are seven or eight confirmed or likely blazars with *synchrotron* flux density brighter than the adopted flux density limit over the considered area. Notwithstanding the uncertainties discussed above and the limited statistics, the H-ATLAS survey allows us to put significant constraints on the 500 μm blazar counts, thus providing a test on evolutionary models and, in consequence, on the underlying physics. For example,

the model by De Zotti et al. (2005) assumes, for all blazars, a flat radio spectral index followed by a parabolic decline above a synchrotron peak frequency that increases with decreasing radio luminosity according to the 'blazar sequence' model (Fossati et al. 1998). On the other hand, Tucci et al. (2011) find that the data favour a broad range of peak frequencies, so broad that any trend with luminosity is blurred. They also argue for different distributions of break frequencies, $\nu_{\rm m}$, for BL Lacs and FSRQs, in the sense that the former objects have substantially higher values of $\nu_{\rm m}$, implying that their synchrotron emission comes from more compact regions. Both points are supported by the study of Giommi et al. (2012).

The De Zotti et al. (2005) model predicts 0.21 blazars deg^{-2} brighter than 35 mJy at 500 μm, i.e. ≃28 blazars over the H-ATLAS Phase 1 area. At the same flux density limit the Tucci et al. (2011) predictions are in the range 0.068–0.12 blazars deg^{-2}, implying about nine to 16 blazars over the Phase 1 area, the lower values referring to the C2Ex model, the higher to the C2Co model. The present analysis shows that the 500 μm blazar counts are substantially below the predictions of the De Zotti et al. (2005) model but consistent with those of the Tucci et al. (2011) models. The most consistent model is the C2Ex, which is also favoured by other data. This adds to the growing evidence (e.g. Planck Collaboration 2011b) that the synchrotron peak frequency of most blazars occurs at lower frequencies than envisaged by the 'blazar sequence' scenario.

Our estimate is also fully consistent with the *Planck* counts of synchrotron extragalactic sources. Planck Collaboration (2012) found, at 545 GHz (550 μm), ≃ 1.5 sources sr^{-1} brighter than 1.2 Jy. Combined with our result, this implies a slope of the integral counts between 1.2 Jy and 35 mJy $\beta \simeq 1.3$–1.4, close to the slope of blazar counts at lower frequencies (see e.g. Tucci et al. 2011).

5 CONCLUSIONS

The sub-mm selection emphasizes blazar flavours that are marginal or missing in the familiar radio or X-ray-selected samples. In the H-ATLAS fields that we have investigated we found nine catalogued blazars with $S_{500\,\mu{\rm m}} \geq 35$ mJy over the area of 134.55 deg^2. To pick out additional blazars that may have been missed in prior surveys new diagnostics need to be devised. The basic selection, based on radio loudness, singled out 12 sources, that could include, in addition to candidate blazars, radio galaxies and steep spectrum radio-loud quasars. To identify candidate blazars we used diagnostics based on optical (SDSS) and on IR (*WISE*) colours, but the possible contamination of the synchrotron emission by the contribution from dust heated by star formation in the host galaxy and from the AGN-related emission (dusty torus and accretion disc) prevented firm conclusions. A better discrimination between the possible classes of sources was obtained from consideration of the full body of available multiwavelength data. Taking also into account the preliminary results of multifrequency follow-up measurements up to ≃40 GHz with the Australia Telescope Compact Array (ATCA), the SED of only one of the 12 selected sources was found to be compatible with being synchrotron dominated at least up to 500 μm, i.e. with being blazar like.

Another object may consist of a faint blazar nucleus inside a bright star-forming galaxy. Although this is at odds with the notion that blazar hosts are passive ellipticals, the possibility that some blazar hosts are endowed with active star formation is supported by our analysis of the SEDs of *Planck* ERCSC blazars detected at both 545 and 857 GHz. The sub-mm continuum of five of the 12 such objects appears to be dominated by thermal dust emission. Also several of these sub-mm-selected blazars with likely star-forming hosts are classified as flat-spectrum radio quasars, although quasar-type blazars are expected to outshine the host galaxy. This situation however is not implausible since the far-IR emission peak associated with star formation can easily outshine the quasar emission at the same wavelength.

The estimated rest-frame synchrotron peak frequencies (in terms of νL_ν) of catalogued blazars are in the range $11.5 \leq \log(\nu_{\rm peak,\,Hz}) \leq 13.7$, with a median $\log \nu_{\rm peak,\,median,\,Hz} \simeq 12.5$. These objects are thus LSPs. Interestingly, the only known blazar in our H-ATLAS sample that happened to be observed twice by *Herschel* (blazar #3), with a time lag of about 6 months, showed a flux increase by a factor of about 60 per cent thus providing direct confirmation of the non-thermal nature of its sub-mm emission.

Six of the catalogued blazars also show evidence of an UV excess that can be attributed to emission from the accretion disc. Under the standard accretion disc model the properties of the excess can be exploited to estimate the black hole mass and the accretion rate. However, these properties are poorly constrained by the available, non-simultaneous, data. Tentative median values of the black hole mass and of the accretion rate are $M_{\rm bh,\,median} \simeq 0.7 \times 10^9\,{\rm M}_\odot$ and $\dot{M}_{\rm bh,median} \simeq 4\,{\rm M}_\odot\,{\rm yr}^{-1}$.

A standard type 1 QSO SED implies that the *WISE* flux densities and a fraction of sub-mm *Herschel*/SPIRE flux densities of these objects (especially at the shorter wavelengths) can be attributed to the dusty torus around the black hole. The QSO contamination may imply that the pure synchrotron component of two of these sources does not reach the chosen 500 μm flux density threshold.

Allowing also for the possibility of misidentifications, we estimate that there are seven to eight pure synchrotron sources brighter than $S_{500\,\mu{\rm m}} = 35$ mJy over the considered area. This is substantially lower than predicted by the De Zotti et al. (2005) model, based on the blazar sequence scenario, but in good agreement with model C2Ex by Tucci et al. (2011), that adopts a broad distribution of synchrotron peak frequencies at all luminosities, which would have the effect of lowering the effective synchrotron peak frequency for the bright sources of interest here.

At this stage all conclusions must be considered as preliminary because of the poor statistics. This will improve as soon as data for the full H-ATLAS survey, covering an area four times larger, will be available. The sub-mm-selected blazar sample will be further augmented by other *Herschel* surveys such as the *Herschel* Multi-tiered Extragalactic Survey (HerMES; HerMES Collaboration 2012) and the *Herschel* Virgo Cluster Survey (HeVICS; Davies et al. 2012). A blazar search on HeVICS data using the approach proposed in this paper is in progress (Baes, private communication). A complementary view of sub-mm-selected blazars is being provided by the *Planck* surveys, which cover the whole sky with detection limits more than an order of magnitude brighter than achieved by the H-ATLAS survey at similar wavelengths.

ACKNOWLEDGEMENTS

The authors would like to thank an anonymous referee for useful comments and suggestions. Partial financial support to this work was provided by the Spanish Ministerio de Economía y Competitividad projects AYA2010-21490-C02-01, AYA2010-21766-C03-01 and CSD2010-00064, by ASI/INAF Agreement I/072/09/0 for the *Planck* LFI activity of Phase E2, by MIUR PRIN 2009 and by INAF through the PRIN 2009 'New light on the early Universe

with sub-mm spectroscopy'. ML-C thanks the Spanish Ministerio de Economía y Competitividad for a Juan de la Cierva fellowship. JG-N thanks the Spanish CSIC for a JAE DOC fellowship.

This research has made use of the NASA/IPAC Extragalactic Database (NED), of SDSS DR8 data and of data products from the *Wide-field Infrared Survey Explorer* (*WISE*).

The NED is operated by the Jet Propulsion Laboratory, California Institute of Technology, under contract with the National Aeronautics and Space Administration. *WISE* is a joint project of the University of California, Los Angeles, and the Jet Propulsion Laboratory/California Institute of Technology, funded by the National Aeronautics and Space Administration.

Funding for SDSS-III has been provided by the Alfred P. Sloan Foundation, the Participating Institutions, the National Science Foundation and the US Department of Energy Office of Science. The SDSS-III web site is www.sdss3.org/. SDSS-III is managed by the Astrophysical Research Consortium for the Participating Institutions of the SDSS-III Collaboration including the University of Arizona, the Brazilian Participation Group, Brookhaven National Laboratory, University of Cambridge, University of Florida, the French Participation Group, the German Participation Group, the Instituto de Astrofísica de Canarias, the Michigan State/Notre Dame/JINA Participation Group, Johns Hopkins University, Lawrence Berkeley National Laboratory, Max Planck Institute for Astrophysics, New Mexico State University, New York University, Ohio State University, Pennsylvania State University, University of Portsmouth, Princeton University, the Spanish Participation Group, University of Tokyo, University of Utah, Vanderbilt University, University of Virginia, University of Washington and Yale University.

REFERENCES

Abdo A. A. et al., 2010, ApJ, 716, 30
Ackermann et al., 2012, ApJ, 743, 171
Aihara H. et al., 2011, ApJS, 193, 29 [Erratum: 2011, ApJS, 195, 26]
Becker R. H., White R. L., Helfand D. J., 1995, ApJ, 450, 559
Chini R., Kruegel E., 1994, A&A, 288, L33
Condon J. J., Anderson M. L., Helou G., 1991, ApJ, 376, 95
Cutri R. M. et al., 2011, Explanatory Supplement to the WISE All-Sky Data Release Products
Davies J. I. et al., 2012, MNRAS, 419, 3505
Dermer C. D., 1995, ApJ, 446, L63
Dermer C. D., Schlickeiser R., 1993, ApJ, 416, 458
De Zotti G., Ricci R., Mesa D., Silva L., Mazzotta P., Toffolatti L., González-Nuevo J., 2005, A&A, 431, 893
Dunlop J. S., Hughes D. H., Rawlings S., Eales S. A., Ward M. J., 1994, Nat, 370, 347
Eales S. et al., 2010, PASP, 122, 49
Fleuren S. et al., 2012, MNRAS, 423, 2407
Fossati G., Maraschi L., Celotti A., Comastri A., Ghisellini G., 1998, MNRAS, 299, 433
Ghisellini G., Tavecchio F., 2009, MNRAS, 397, 985
Giommi P. et al., 2012, A&A, 541, A160
González-Nuevo J. et al., 2010, A&A, 518, L38
Griffin M. J. et al., 2010, A&A, 518, L3
Haardt F., Madau P., 2012, ApJ, 746, 125
Hardcastle M. J. et al., 2010, MNRAS, 409, 122
Helou G., Soifer B. T., Rowan-Robinson M., 1985, ApJ, 298, L7
HerMES Collaboration, 2012, preprint (arXiv:1203.2562)
Herranz D. et al., 2013, A&A, 549, 31
Ibar E. et al., 2010, MNRAS, 409, 38
Ivison R. J. et al., 2010, MNRAS, 402, 245
Jarvis M. J. et al., 2010, MNRAS, 409, 92
Kotilainen J. K., Falomo R., Scarpa R., 1998, A&A, 332, 503
Kotilainen J. K., Falomo R., Labita M., Treves A., Uslenghi M., 2007, ApJ, 660, 1039
Larson D. et al., 2011, ApJS, 192, 16
León-Tavares J., Valtaoja E., Chavushyan V. H., Tornikoski M., Añorve C., Nieppola E., Lähteenmäki A., 2011, MNRAS, 411, 1127
McCarthy P. J., 1993, ARA&A, 31, 639
Mangum J. G., Emerson D. T., Greisen E. W., 2007, A&A, 474, 679
Massaro F., D'Abrusco R., Ajello M., Grindlay J. E., Smith H. A., 2011a, ApJ, 740, L48
Massaro F., Paggi A., Cavaliere A., 2011b, ApJ, 742, L32
Massaro E., Giommi P., Leto C., Marchegiani P., Maselli A., Perri M., Piranomonte S., 2011c, Multifrequency Catalogue of Blazars, 3rd edn. Aracne Ed., Rome, Italy
Massaro E., Nesci R., Piranomonte S., 2012, MNRAS, 422, 2322
Netzer H. et al., 2007, ApJ, 666, 806
Nieppola E., Tornikoski M., Valtaoja E., 2006, A&A, 445, 441
O'Dowd M., Urry C. M., 2005, ApJ, 627, 97
Padovani P., Giommi P., 1995, ApJ, 444, 567
Padovani P., Giommi P., Abraham P., Csizmadia S., Moór A., 2006, A&A, 456, 131
Pascale E. et al., 2011, MNRAS, 415, 911
Perlman E., Addison B., Georganopoulos M., Wingert B., Graff P., 2008, in Proc. Workshop on Blazar Variability Across the Electromagnetic Spectrum. Published online at http://pos.sissa.it, p. 9
Pilbratt G. L. et al., 2010, A&A, 518, L1
Planck Collaboration, 2011a, A&A, 536, A7
Planck Collaboration, 2011b, A&A, 536, A13
Planck Collaboration, 2012, preprint (arXiv:1207.4706)
Plotkin R. M., Anderson S. F., Brandt W. N., Markoff S., Shemmer O., Wu J., 2012, ApJ, 745, L27
Poglitsch A. et al., 2010, A&A, 518, L2
Polletta M. et al., 2007, ApJ, 663, 81
Procopio P. et al., 2011, MNRAS, 417, 1123
Rigby E. E. et al., 2011, MNRAS, 415, 2336
Righini S., 2008, IRA Internal Report 425/08
Silva L., Granato G. L., Bressan A., Danese L., 1998, ApJ, 509, 103
Smith D. et al., 2012, MNRAS, 427, 703
Swinyard B. M. et al., 2010, A&A, 518, L4
Tramacere A., Massaro E., Taylor A. M., 2011, ApJ, 739, 66
Tucci M., Toffolatti L., de Zotti G., Martínez-González E., 2011, A&A, 533, A57
Wright E. L. et al., 2010, AJ, 140, 1868

This paper has been typeset from a TEX/LATEX file prepared by the author.